

Segmented Waves from a Spatiotemporal Transverse Wave Instability

Lingfa Yang, Igal Berenstein, and Irving R. Epstein*

Department of Chemistry and Volen Center for Complex Systems, MS 015, Brandeis University, Waltham, Massachusetts 02454-9110, USA

(Received 14 March 2005; published 14 July 2005)

We observe traveling waves emitted from Turing spots in the chlorine dioxide-iodine-malonic acid reaction. The newborn waves are continuous, but they break into segments as they propagate, and the propagation of these segments ultimately gives rise to spatiotemporal chaos. We model the wave-breaking process and the motion of the chaotic segments. We find stable segmented spirals as well. We attribute the segmentation to an interaction between front rippling via a transverse instability and front symmetry breaking by a fast-diffusing inhibitor far from the codimension-2 Hopf-Turing bifurcation, and the chaos to a secondary instability of the periodic segmentation.

DOI: [10.1103/PhysRevLett.95.038303](https://doi.org/10.1103/PhysRevLett.95.038303)

PACS numbers: 82.40.Ck, 47.54.+r, 89.75.Kd

Spiral waves and, more generally, traveling waves have been thoroughly studied in excitable and oscillatory media. In most of these active media, the inhibitor species diffuses at a rate comparable to or less than the activator, or is immobilized, and the wave fronts are continuous and stable. When waves in the Belousov-Zhabotinsky (BZ) reaction lose stability, they exhibit ripples or break up due to wave front instability [1]. Spiral breakup was also reported in the BZ reaction due to convective instability [2]. This form of breakup has been discussed in connection with the mechanism of cardiac fibrillation [3]. In systems where the inhibitor diffuses more rapidly than the activator, breakup is associated with a negative eikonal-curvature relation [4,5]. Spiral breakup typically leads to spiral turbulence or chaotic waves [6], except for a recent report of stable segmented spirals in the BZ-AOT [AOT = sodium bis(2-ethylhexyl) sulfosuccinate] microemulsion system [7]. In most cases of unstable waves, a faster-diffusing inhibitor plays a key role, a phenomenon which has drawn much attention recently. In fast inhibitor systems, fronts separating bistable steady states can show interesting behavior as well, developing into labyrinthine patterns [8] or cellular structures [9–11], both of which show intrinsic wavelengths.

Here, we examine waves in the chlorine dioxide-iodine-malonic acid (CDIMA) reaction, where the activator species is iodide, which diffuses slowly or is immobilized, due to the presence of a complexing agent in the gel medium. The chlorite inhibitor, in contrast, diffuses rapidly. This condition favors Turing instability, and it was in this system that Turing's idea [12] was first brought to experimental reality [13]. The coexistence between Turing patterns and waves has been observed previously as superposed [14] or juxtaposed [15] patterns, or as mixed turbulence [14] near a codimension-2 Turing-Hopf bifurcation point. Here, we report a different coexistence, far above the codimension-2 point, where the Turing structures serve as wave sources, and the continuous waves are unstable and break into segments; spirals separate into segmented spirals while preserving the striking spiral envelope. The

segmentation does not settle down with a unique perforation length. Instead, segments keep growing, splitting, shrinking, and vanishing in a “staggering” motion. We simulate these behaviors with a simple reaction-diffusion model, analyze the stability properties of this segmentation to find the relevant transverse spatiotemporal wave front instability, and calculate the dispersion relation.

Our experiments are carried out in a one side fed unstirred reactor. The working medium is an agarose gel (2%, Fluka), which is separated from the feeding chamber by an Anapore membrane (Whatman, pore size $0.2 \mu\text{m}$) impregnated with agarose gel (4%) to avoid stirring effects and a cellulose nitrate membrane (Whatman, pore size $0.45 \mu\text{m}$) for contrast. Three solutions are fed into the reactor, one containing I_2 (Aldrich), another ClO_2 , and the third malonic acid (MA, Aldrich) and poly (vinyl alcohol) (PVA, Aldrich, 80% hydrolyzed, average mol. wt. 9000–10 000), all prepared in a 10 mM solution of sulfuric acid [16].

Figures 1(a)–1(c) show a sequence of snapshots of segmented waves emitted from Turing spots or outwardly propagating spirals. Initially the system shows continuous waves that move rapidly, but as the concentration of PVA

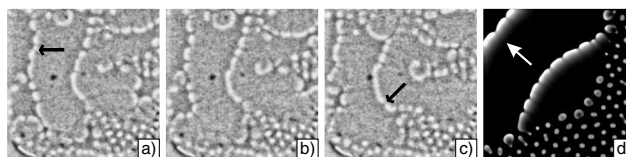


FIG. 1. Segmented waves in the CDIMA reaction (a),(b),(c). Frame (b) taken 50 s after frame (a), and frame (c) taken 115 s after (b). The spot pointed to by the arrow in (a) disappears in (b), while the arrow in (c) signals the segmentation of a wave. Frame size $15 \times 15 \text{ mm}^2$. $[\text{I}_2]_0 = 0.36 \text{ mM}$, $[\text{MA}]_0 = 1.85 \text{ mM}$, $[\text{ClO}_2]_0 = 0.14 \text{ mM}$, $[\text{poly(vinyl-alcohol)}] = 0.85 \text{ g/L}$. Temperature inside the reactor is 4°C ; residence time is 220 s. Segmented waves represent a transient from traveling waves to Turing patterns. (d) Snapshot from a 2D simulation, size $128 \times 128 \text{ s.u.}$, showing segmented waves generated from Turing spots (see [24] for a movie).

inside the gel rises, Turing patterns appear at the boundaries, and the waves begin to segment. Propagating wave segments exhibit a preferred length, as breaking and vanishing occur frequently. Eventually, the Turing pattern dominates the entire system. Slightly lowering the PVA concentration (to 0.8 g/L) leads to a mixture of waves and Turing patterns that can last for more than 50 h without any domain expanding. For even lower concentrations of PVA, the waves expand, and the Turing patterns disappear.

The Lengyel-Epstein model [17] reproduces Turing patterns in the CDIMA reaction nearly quantitatively [18]. It also yields phase waves and bulk oscillations after a Hopf bifurcation, but it does not support trigger waves, because the model does not display excitability. For a phenomenological description of segmented waves, we therefore choose the well-known Brusselator model [19]:

$$\frac{\partial u}{\partial t} = a - (b + 1)u + u^2v + D_u \nabla^2 u, \quad (1)$$

$$\frac{\partial v}{\partial t} = bu - u^2v + D_v \nabla^2 v. \quad (2)$$

We focus on the fast inhibitor case with diffusion coefficient ratio $\delta = D_u/D_v < 1$. The system has Turing and Hopf bifurcations located at $b_c^T = (1 + a\sqrt{\delta})^2$, and $b_c^H = 1 + a^2$, respectively. The codimension-two Turing-Hopf point occurs where these curves intersect: $a^{TH} = \frac{2\sqrt{\delta}}{1-\delta}$, $b^{TH} = (\frac{1+\delta}{1-\delta})^2$. We fix $D_u = 5$, $D_v = 12$ s.u.²/t.u. (s.u. = space units, t.u. = time units), which puts the codimension-2 point at $(a, b)^{TH} = (2.213, 5.898)$. We take $(a, b) = (2.3, 20)$ for all of our simulations. This large value of b places the system far above both the Turing and Hopf bifurcations ($b \gg b_c^T, b_c^H$), i.e., far from the steady state equilibrium, and with quite nonsinusoidal oscillations supporting trigger waves. With these parameters, we are

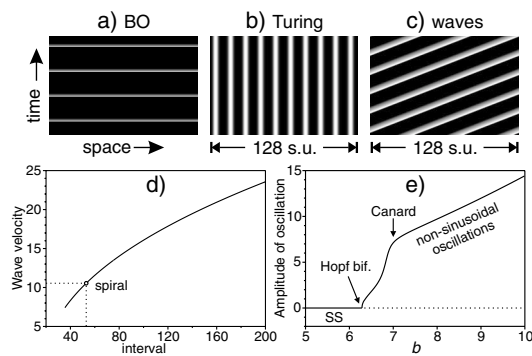


FIG. 2. Three stable solutions from 1D simulations under periodic boundary conditions, size 128 s.u. (a) Bulk oscillation, period $T = 28.8$ t.u.; (b) stationary Turing pattern, wavelength $\lambda_T = 12.8$ s.u.; (c) wave train, propagation velocity $v = 8.9$ s.u./t.u. (d) propagation velocity vs interwave interval in wave trains. Velocity at interval 53 is marked for the archimedean spiral in Fig. 4(c). (e) Amplitude of bulk oscillations increases with b .

able to mimic all the experimental behaviors described above. In Fig. 1(d), for example, we demonstrate the coexistence of Turing patterns and segmented waves.

First, we seek all stable solutions in the 1D spatially extended system. When the steady state loses stability, one of the solutions is bulk oscillation (BO). The stability of BO can be evaluated by calculating the Floquet multipliers [20]. We find that the two Floquet multipliers decrease quickly to zero as the wave number increases, which means that BO is stable toward infinitesimal spatial perturbations.

In addition to the single homogeneous BO solution, there are two inhomogeneous solutions: Turing patterns and wave trains. Both are stable in the Lyapunov sense. These three solutions are shown in Figs. 2(a)–2(c).

Because both solutions are stable, Turing patterns can coexist with waves [Figs. 1(a)–1(c)], leading to competition. In the experiments in Fig. 1, the coexistence is a transient in the evolution toward Turing patterns; i.e., the Turing solution is more stable than the wave solution. With our chosen parameters the model yields the same behavior [Fig. 1(d)], but the situation can be reversed by a different choice of parameters, as occurs in the experiments. Competition between Turing patterns and bulk oscillations near the codimension-2 Turing-Hopf point was studied using a weakly nonlinear analysis in Ref. [21], but such techniques fail far from this point, where excitation wave solutions can arise.

We are more interested in the wave solution. The wave velocity depends on the recovery of the medium and its excitation, which are related to the interval between successive waves. We calculate this relation in Fig. 2(d), and find that a sparse wave train with a large interval can move as much as five times faster than a dense wave train. Slow waves are trigger waves, which arise after a canard [Fig. 2(e)]; they tend to break into segments in 2D.

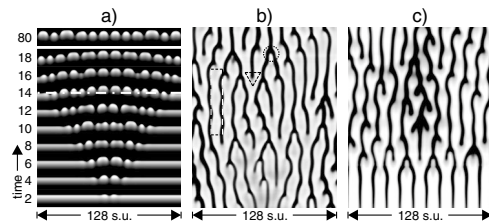


FIG. 3. Formation of a segmented wave and its motion in 2D simulations, size 128×43 s.u., periodic boundary conditions. (a) Discrete snapshots show a smooth continuous traveling wave breaking up into wave segments. (b) Space-time plot of a continuous run from (a) in the time window $t = 3370$ – 3430 t.u. showing spatiotemporal chaos in the comoving frame at velocity $v = 9.15$ t.u./s.u. Marked areas show splitting (triangle), vanishing (circle), and breathing (rectangle). (c) Secondary instability destabilizes periodic segmented waves into chaos. Spatiotemporal plot in the comoving frame, $t = 20$ – 80 t.u. (see [24] for a movie).

To demonstrate the wave-breaking behavior, we carry out a 2D simulation in Fig. 3(a), where a small local concentration perturbation is added at the middle of a smooth continuous traveling wave. The local perturbation grows and causes the first break at 2 t.u. The following snapshots show the spreading of the perturbation and the breaking of the continuous wave into segments. Here the segmented portion of the wave moves slightly faster than the continuous portion, resulting in the convex envelope seen at 14 t.u., where the horizontal dash-dot line emphasizes that the segmented part is ahead of the continuous part. As the segmented wave propagates, however, the convex curvature finally disappears, as shown at 80 t.u.

The segmented wave shows a preferred wavelength (segment length plus gap, with the gap maintaining nearly constant length), $\lambda_0 = 11.6$ s.u. If a segment is longer than λ_0 it may split or shrink. Shorter segments may grow, or simply disappear. This dynamics might be expected to lead eventually to a unique segment length. Instead, we observe a staggering motion as shown in Fig. 3(b), which results in spatiotemporal chaos.

To confirm that the system does not evolve to a stationary periodic front, we followed a long run up to $t = 4000$ t.u. in Fig. 3(b). More convincingly perhaps, we performed another simulation where the system was initialized at the perforation wavelength. Figure 3(c) shows that the periodic segmented wave is not stable and deteriorates into the staggering motion within 50 t.u., indicating the existence of a secondary instability.

Figures 4(a)–4(c) demonstrate that a planar continuous wave with one free end can roll up and transform into a stable segmented spiral wave. Figure 4(d) shows superimposed snapshots taken over one full rotation period. The spiral tip is a singularity, shown as a bright spot. Close to the tip, the wave has smaller amplitude and looks darker. Segments, seen as ripples, are sparser and shallower close to the tip area, and increase in frequency and depth as we move out from the center. Clearly, there is a threshold of length, above which one segment breaks into two. We also observe some segments vanishing during propagation. In the presence of spatial noise, more break points are seeded,

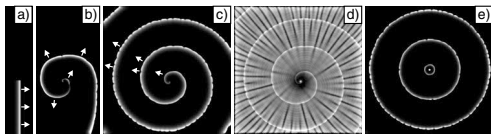


FIG. 4. Segmented spiral wave develops from a continuous traveling wave with a free end subject to spatial random noise ($< 1.4\%$). Arrows indicate propagation directions. System size 256×256 s.u. (a) Initial wave ($t = 0$); (b) spiral begins to develop ($t = 10$). (c) Developed segmented spiral ($t = 30$). (d) Twenty-six superimposed snapshots in one period $T = 5$ t.u. The spiral tip is located at the white spot. (e) Segmented target pattern arising from a “dust” ($u = 10$, $v = 8.7$) (see [24] for a movie).

so that segmentation becomes easier and spreads more rapidly than in a noise-free system. A target pattern formed in this way is shown in Fig. 4(e).

Why does a continuous spiral break up into segments? Our spiral is archimedean, $r = a\varphi$ in polar coordinates, with position-dependent curvature κ given by $\frac{2+\varphi^2}{a(1+\varphi^2)^{3/2}}$, where $a = 53/2\pi$. Recall Fig. 3(a) where a planar wave (zero-curvature) can break up as well, which indicates that the profiles’ curvature is not the cause of segmentation. Note also, that after segmentation the local curvatures of the segments vary, but they all propagate at the same velocity, so that the profile is preserved. This feature distinguishes our segmented spirals from spiral turbulence [6], where propagation failure and reversal of propagation direction (backfiring) can be found, and the segmentation can be traced back to eikonal-curvature effects [22], which are not relevant here.

Though the segmentation of this spiral resembles that seen in the BZ-AOT system [7], these phenomena have distinct mechanisms. Segmented spirals [7], as well as “dash waves” [23], in the BZ-AOT system, are believed to emerge from the interaction between two steady states, “one of which is excitable, whereas another is pseudo-Turing unstable.” Here, the system has a single steady state, which does not show “pseudo-Turing instability” [23]. Moreover, our segmented waves, either as a planar envelope in Fig. 3(a) or as a rotating spiral in Fig. 4(c), emerge from traveling waves. Therefore the analysis should utilize the wave solution rather than the steady state solution. Our phase wave trains (limit cycles) lie far from the steady state and are quite nonsinusoidal, so that any analysis based on the steady state solution is likely to fail.

Our stability analysis starts from a planar wave front solution. We consider an infinitesimal sinusoidal perturbation along the front. By inserting this solution into the reaction-diffusion equations, and linearizing about the planar front in a comoving frame, the problem is transformed into an inhomogeneous eigenvalue problem. The dispersion can be obtained numerically from the solvability condition [9]. We calculate the dispersion by direct simulations on a system of size 128×43 s.u. with mesh

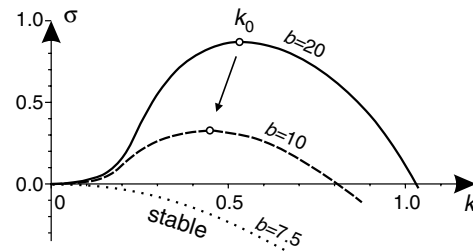


FIG. 5. Dispersion relation of traveling wave transverse instability for Fig. 3 (solid line). Decreasing b lowers the growth rate and shifts to the left the most positive wave number (dashed line), until the instability vanishes (dotted line).

0.25 s.u. using an explicit Euler integration step 1.0×10^{-4} t.u., and show the result in Fig. 5. The most unstable mode lies at $k_0 = 0.53$, or wavelength $\lambda_0 = 12$ s.u., which agrees very well with the perforation wavelength for segmentation in Figs. 3 and 4. Decreasing b decreases the excitability, which vanishes around $b = 7$, and weakens the transverse instability.

When a wave front loses stability via a transverse instability, it becomes sinusoidally modulated (rippled). This modulation remains symmetric at small amplitude, and the concentration along the front is constant. As the amplitude grows, symmetry is lost, and the concentration of activator at the valleys (lagging regions of the propagating front) becomes lower than at the crests (leading portions) due to annihilation from the fast-diffusing inhibitor. This concentration difference creates the perception that a continuous wave front has broken into segments. Therefore, the segmentation phenomenon is a combination of geometric curve rippling and symmetry breaking of the uniform concentration profile along the front. If we change the diffusivity, propagation failure can occur at the valleys, which either produces stationary Turing spots or generates new waves propagating in the opposite direction (back-firing). The first case results in the formation of Turing patterns, while the latter case gives breakup to wave segment turbulence (strong chaos).

The staggering motion remains an open question. If we define the primary instability as the wave front instability that gives rise to periodic segmentation, then secondary instabilities refer to the loss of stability of the segmented structure. We note that the unstable sideband in Fig. 5 is quite broad, which allows a rich array of harmonic modes. We speculate that the interaction among the most unstable mode at k_0 and modes in this sideband causes the staggering motion of propagating segmented waves, resulting in spatiotemporal chaos (soft chaos).

We have reported observations of segmented waves in the CDIMA reaction under conditions where both Turing patterns and wave solutions are stable and can coexist. Waves are generated from Turing spots or from spiral tips. They break down into segments during propagation, initially maintaining their envelope, rather than degenerating into chaos as is often observed. Our segmentation originates from a spatiotemporal transverse instability of the wave solution, which causes the front first to ripple and then to exhibit large variations in concentration along its length. The dispersion relation analysis shows that the most unstable mode agrees very well with the segmentation length scale. We do not fully understand why the system does not settle at the perforation wavelength, but instead undergoes the staggering motion that ultimately leads to spatiotemporal chaos.

We thank A.M. Zhabotinsky, V.K. Vanag, and M. Dolnik for helpful discussions. This work was supported

by Grant No. CHE-0306262 from the National Science Foundation.

*Electronic address: epstein@brandeis.edu

- [1] M. Markus, G. Kloss, and I. Kusch, *Nature (London)* **371**, 402 (1994).
- [2] Q. Ouyang and J.-M. Flesselles, *Nature (London)* **379**, 143 (1996).
- [3] A. T. Winfree, *Science* **266**, 1003 (1994); A. V. Panfilov and P. Hogeweg, *Science* **270**, 1223 (1995).
- [4] Y. Kuramoto, *Prog. Theor. Phys.* **63**, 1885 (1980).
- [5] A. F. M. Mare and A. V. Panfilov, *Phys. Rev. Lett.* **78**, 1819 (1997).
- [6] A. Hagberg and E. Meron, *Phys. Rev. Lett.* **72**, 2494 (1994); *Phys. Rev. E* **57**, 299 (1998); E. Meron *et al.*, *Catal Today* **70**, 331 (2001).
- [7] V.K. Vanag and I.R. Epstein, *Proc. Natl. Acad. Sci. U.S.A.* **100**, 14635 (2003).
- [8] K.J. Lee, W.D. McCormick, Q. Ouyang, and H.L. Swinney, *Science* **261**, 192 (1993); K.J. Lee and H.L. Swinney, *Phys. Rev. E* **51**, 1899 (1995).
- [9] D. Horváth, V. Petrov, S.K. Scott, and K. Showalter, *J. Chem. Phys.* **98**, 6332 (1993).
- [10] É. Jakab, D. Horváth, and A. Tóth, *Phys. Chem. Chem. Phys.* **4**, 1307 (2002); Z. Virányi, A. Szommer, A. Tóth, and D. Horváth, *Phys. Chem. Chem. Phys.* **6**, 3396 (2004).
- [11] M. Fuentes, M. N. Kuperman, and P. De Kepper, *J. Phys. Chem. A* **105**, 6769 (2001).
- [12] A.M. Turing, *Phil. Trans. R. Soc. B* **237**, 37 (1952).
- [13] V. Castets, E. Dulos, J. Boissonade, and P. De Kepper, *Phys. Rev. Lett.* **64**, 2953 (1990); Q. Ouyang and H.L. Swinney, *Nature (London)* **352**, 610 (1991).
- [14] B. Rudovics, E. Dulos, and P. De Kepper, *Phys. Scr.* **T67**, 43 (1996); J. Boissonade, E. Dulos, and P. De Kepper, in *Chemical Waves and Patterns*, edited by R. Kapral and K. Showalter (Kluwer, Dordrecht, 1995), p. 221.
- [15] J.-J. Perraud *et al.*, *Phys. Rev. Lett.* **71**, 1272 (1993).
- [16] I. Berenstein, M. Dolnik, L. Yang, A. M. Zhabotinsky, and I. R. Epstein, *Phys. Rev. E* **70**, 046219 (2004).
- [17] I. Lengyel and I. R. Epstein, *Science* **251**, 650 (1991).
- [18] B. Rudovics *et al.*, *J. Phys. Chem. A* **103**, 1790 (1999).
- [19] I. Prigogine and R. Lefever, *J. Chem. Phys.* **48**, 1695 (1968).
- [20] P. Hartman, *Ordinary Differential Equations* (Wiley, New York, 1964), p. 60.
- [21] M. Or-Guil and M. Bode, *Physica A (Amsterdam)* **249**, 174 (1998).
- [22] C. Elphick, A. Hagberg, and E. Meron, *Phys. Rev. E* **51**, 3052 (1995); A. Hagberg *et al.*, *Phys. Rev. E* **55**, 4450 (1997).
- [23] V. K. Vanag and I. R. Epstein, *Phys. Rev. Lett.* **90**, 098301 (2003).
- [24] Movies of these dynamic patterns are available at <http://hopf.chem.brandeis.edu/yanglingfa/pattern/seg/index.html>.